



**HAL**  
open science

## **pH-Switchable Stratification of Colloidal Coatings: Surfaces “On Demand”**

Ignacio Martín-Fabiani, Andrea Fortini, Jennifer Lesage de La Haye, Ming Liang Koh, Spencer Taylor, Elodie Bourgeat-Lami, Muriel Lansalot, Franck D’agosto, Richard Sear, Joseph Keddie

► **To cite this version:**

Ignacio Martín-Fabiani, Andrea Fortini, Jennifer Lesage de La Haye, Ming Liang Koh, Spencer Taylor, et al.. pH-Switchable Stratification of Colloidal Coatings: Surfaces “On Demand”. ACS Applied Materials & Interfaces, 2016, 8 (50), pp.34755 - 34761. 10.1021/acsami.6b12015 . hal-01859555

**HAL Id: hal-01859555**

**<https://hal.science/hal-01859555>**

Submitted on 22 Dec 2021

**HAL** is a multi-disciplinary open access archive for the deposit and dissemination of scientific research documents, whether they are published or not. The documents may come from teaching and research institutions in France or abroad, or from public or private research centers.

L’archive ouverte pluridisciplinaire **HAL**, est destinée au dépôt et à la diffusion de documents scientifiques de niveau recherche, publiés ou non, émanant des établissements d’enseignement et de recherche français ou étrangers, des laboratoires publics ou privés.

# pH-Switchable Stratification of Colloidal Coatings: Surfaces “On Demand”

Ignacio Martín-Fabiani,<sup>a,†</sup> Andrea Fortini,<sup>a</sup> Jennifer Lesage de la Haye,<sup>b</sup> Ming Liang Koh,<sup>b</sup> Spencer E. Taylor,<sup>c</sup> Elodie Bourgeat-Lami,<sup>b</sup> Muriel Lansalot,<sup>b</sup> Franck D’Agosto,<sup>b</sup> Richard P. Sear<sup>a</sup> and Joseph L. Keddie<sup>\*,a</sup>

a. Department of Physics, University of Surrey, Guildford, Surrey GU2 7XH, United Kingdom

b. Univ Lyon, Université Claude Bernard Lyon 1, CPE Lyon, CNRS, UMR 5265, Chemistry, Catalysis, Polymers and Processes (C2P2), 43 Bd du 11 Novembre 1918, 69616 Villeurbanne, France

c. Centre for Petroleum and Surface Chemistry, Department of Chemistry, University of Surrey  
GU2 7XH Guildford, Surrey GU2 7XH, United Kingdom

**KEYWORDS.** *stimuli-responsive; polymerization-induced self-assembly (PISA); functional coatings; stratification; Brownian dynamics simulations*

---

**ABSTRACT:** Stratified coatings are used to provide properties at a surface, such as hardness or refractive index, which are different from underlying layers. Although time-savings are offered by self-assembly approaches, there have been no methods yet reported to offer stratification on demand. Here, we demonstrate a strategy to create self-assembled stratified coatings, which can be switched to homogenous structures when required. We use blends of large and small colloidal polymer particle dispersions in water that self-assemble during drying because of an osmotic pressure gradient that leads to a downward velocity of larger particles. Our confocal fluorescent microscopy images reveal a distinct surface layer created by the small particles. When the pH of the initial dispersion is raised, the hydrophilic shells of the small particles swell substantially, and the stratification is switched off. Brownian dynamics simulations explain the suppression of stratification when the small particles are swollen as a result of reduced particle mobility, a drop in the pressure gradient, and less time available before particle jamming. Our strategy paves the way for applications in antireflection films and protective coatings in which the required surface composition can be achieved on demand, simply by adjusting the pH prior to deposition.

---

**Introduction.** Stratified coatings, consisting of two or more layers on top of each other, are used in a wide range of applications, including energy storage,<sup>1</sup> optics,<sup>2</sup> biomedicine,<sup>3</sup> and photovoltaics.<sup>4</sup> The development of fast, inexpensive, and up-scalable fabrication methods for stratified systems is a key challenge in materials science.<sup>5</sup> <sup>6</sup> Here, we introduce a method to obtain self-assembled stratified coatings, along with a simple means to form homogeneous coatings, when desired, using the same starting materials.

The casting of polymer blends from a common solvent provides one of the simplest fabrication methods. Stratified coatings can evolve from the growth of wetting layers at the surface, driven by differences in surface free energies between the two phases.<sup>7</sup> A three-layer lamellar structure has been reported in solvent-cast polymer binary blends.<sup>8</sup> During spin-casting from solvent, stratified layers develop as a transient stage sometimes followed by lateral phase separation.<sup>9, 10</sup> A limitation when forming stratified coatings by solvent casting is that the final com-

position depth profile can only be adjusted by changing the polymer's surface energy, molecular weights, or chain architecture.

Colloidal self-assembly methods, using *particles* suspended in a solvent as the building blocks, rather than single molecules, have been proposed as single-step alternatives for producing stratified coatings, via the control of colloidal particle diffusion,<sup>11, 12</sup> sedimentation,<sup>13</sup> particle interaction potentials,<sup>14</sup> or surface free energy.<sup>15</sup> We recently discovered a mechanism of self-stratification in blends of colloids of two different sizes, where the small particles segregate into a layer on top of the larger particles.<sup>16</sup> When drying a blend of colloidal particles in a liquid, the top interface of the liquid falls as a result of evaporation, and an osmotic pressure gradient develops across the thickness of the layer. This pressure gradient pushes larger particles away from the air-liquid interface faster than it pushes smaller particles, creating stratification. Although examples of stratification by particle size can be found in the literature,<sup>17</sup> no suitable physical model existed at that time to explain the effect.

To fulfill the aspirations of materials scientists for designer materials, there is a demand that the stratification of a coating is responsive, such that it can be switched on and off as needed, or varied between set limits. There is currently a gap in existing technologies to offer a combination of stratification and switchability to yield surface properties "on demand". For instance, in applications as a protective coating, the surface might need a higher hardness<sup>17</sup> to impart scratch-resistance. In antireflection coatings, a lower refractive index at the surface will reduce the optical reflectivity.<sup>18</sup> Gradients in composition suppress reflection losses significantly, in a broad bandwidth and under diffuse illumination.<sup>19</sup> A means to adjust stratification without altering the starting composition or the deposition method would offer a huge efficiency gain over conventional fabrication technology.<sup>6, 20-22</sup>

Our vision in the design of a switchable, stratified coating is to draw upon insights from our earlier work<sup>23</sup> to bring together two different materials technologies: colloidal stratification and pH-responsive particles. Here, we show how the stratification of binary particle blends can be switched off (or on) simply by raising (or lowering) the pH of the initial dispersion. Using stimuli-responsive polymer colloids that increase in size when the pH is raised, the driving force for segregation during drying is reduced enough to suppress stratification. Thus, without changing the composition of the materials, the properties of the surface layer and bulk film are manipulated on demand. We envision that our design will allow end-users to define the properties of the final coating via a pH adjustment before deposition. To this end, we present a proof of concept of a new class of coating that offers a function beyond the ordinary.

In our previous work, we observed that stratification in binary colloidal blends becomes less efficient either when the initial solids content is increased or when the size ratio of the particles is reduced.<sup>16, 24</sup> To exploit this behavior, we employ switchable or responsive polymers, which

are ideal platforms because of their ability to respond to a variety of external stimuli, *e.g.* temperature, light or pH, with conformational and/or chemical changes.<sup>25</sup> This versatility makes them a key part of advances in drug delivery,<sup>26</sup> sensors,<sup>27</sup> and nano- and microactuation.<sup>28</sup>

Via emulsion polymerization,<sup>29, 30</sup> polymer particles can be synthesized with a dense polymer core on which hydrophilic polymer chains, referred to as hairy layers, are anchored to create a shell.<sup>31</sup> Raising the pH can be used to increase the hydrophilicity of the hairy layer, and hence to increase the effective size of the particles.<sup>32</sup> In this work, we use the recently-developed method of polymerization-induced self-assembly (PISA) to synthesise particles with pH-responsive hairy layers as a means to adjust the particle size.<sup>33-35</sup>

PISA combines emulsion polymerization and reversible deactivation radical polymerization (RDRP) concepts to produce surfactant-free latexes. The process requires the synthesis by RDRP of hydrophilic polymer chains followed by their chain extension with a hydrophobic monomer in water leading to the formation of amphiphilic block copolymers. The hydrophilic segment covalently anchored at the particle surface will ensure the stabilization.

**Results.** PISA was employed to synthesize copolymer particles composed of styrene and acrylate derivatives and stabilized by poly(methacrylic acid) (PMAA). These particles are pH-responsive, as the PMAA chains on their surfaces will be protonated at low pH. Protonation reduces the charge and thus causes chain collapse at a pH below the pKa. When the pH is raised, these chains are deprotonated and extend as their affinity with water increases, as shown in Figure 1. The particle hydrodynamic diameter, as measured by dynamic light scattering (DLS), increases with increasing pH, as is shown in Figure 2a. At pH 9.5, the effective diameter of the small particles is almost double that at pH 4. Another clear sign of the increase in particle size can be seen from the pH dependence of the viscosity of a dispersion of these particles (at a fixed concentration of 20 wt% solids). As shown in Figure 2b, there is a remarkable increase in viscosity above pH 5.

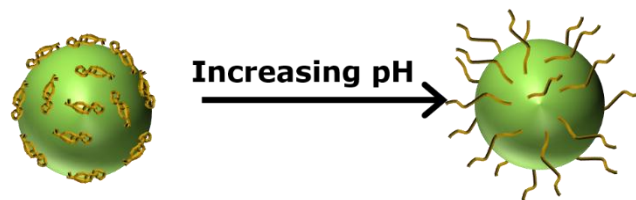


**Figure 1. Effects of pH on hairy-layer PISA particles: Scheme depicting the extension of PMAA chains at the particle surface when the pH of the initial dispersion is raised.**

The viscosity dependence on the particle volume fraction (adjusted through the pH) is presented in Figure 2c. Here, an effective volume fraction of particles,  $\phi_{\text{eff}}$ , was calculated using the number density of the particles and the diameters obtained from DLS for a particular pH. (At

20 wt%, the number density is  $2.4 \times 10^{21}/\text{m}^3$  for the small particles and  $6.0 \times 10^{18}/\text{m}^3$  for the large particles.) A general trend for the viscosity to increase with increasing  $\phi_{\text{eff}}$  is observed, with the exception of the viscosity at the highest  $\phi_{\text{eff}}$ , where a decrease is observed.

For comparison, the prediction of the Krieger-Dougherty model<sup>36</sup> for the viscosity of hard colloidal spheres is shown in Figure 2c. There is poor agreement. However, because the diffuse shell of the particles is made of swollen PMAA chains, the particles cannot be treated as hard spheres at high densities. Instead, the hairy layer shells can interact with and interpenetrate neighboring shells, which causes the dispersion viscosity to be large but finite. The observed trend differs from that seen with hard particles jamming, which causes the viscosity to diverge towards infinity. Thus, the rapidly increasing but non-diverging viscosity seen in Figure 2c is as is expected for swollen, soft spherical particles. As the viscosity increases, the particle mobility, which is essential for stratification, decreases.

The pH-responsive particles, with a size at low pH of approximately 50 nm, were labeled with fluorescein for confocal microscopy experiments. In stratification experiments, they were blended with larger particles (385 nm), synthesized via a conventional emulsion polymerization process using surfactant as a stabilizer and labeled with a red fluorescent dye (Rhodamine B). These large red particles show no significant changes in size (Figure S1) or viscosity (Figures 2b and S3) with increasing pH.

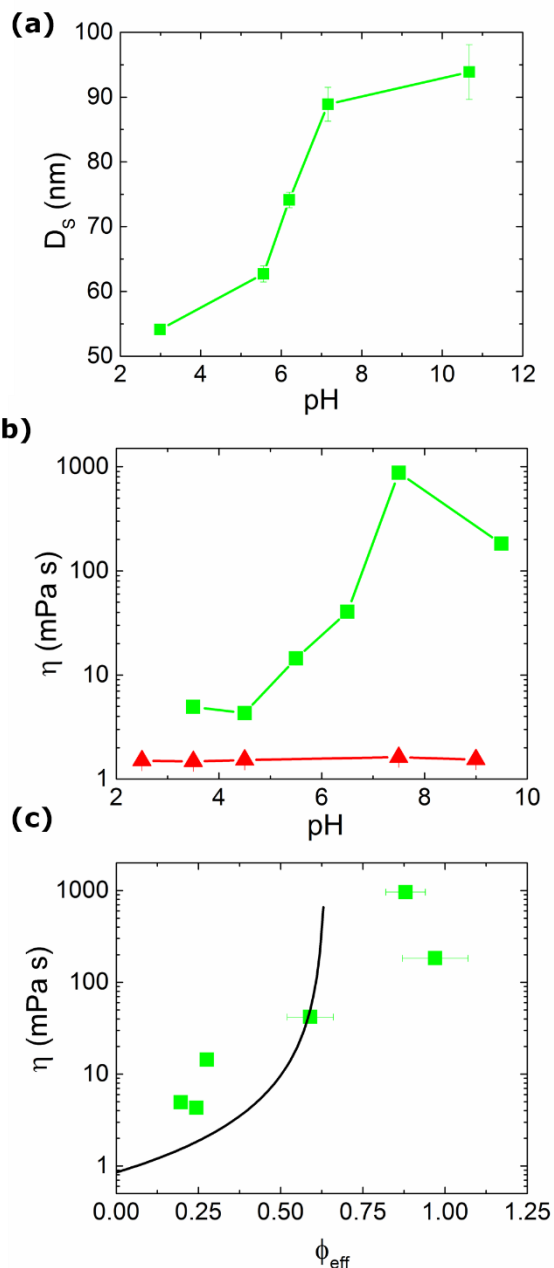


**Figure 2.** Effects of pH on hairy-layer PISA particles. (a) Particle diameters measured by dynamic light scattering as a function of pH. (b) Viscosity at a shear rate of  $2.4 \text{ s}^{-1}$  as a function of the dispersion pH. The number density of particles is constant across the series (corresponding to 20 wt%). For comparison, the dependence of the viscosity of large (385 nm) emulsion polymer particles at 20 wt% is plotted (red triangles). (c) Viscosity of dispersions of pH-responsive particles (as in b) replotted as a function of their effective volume fraction,  $\phi_{\text{eff}}$ , as the pH is raised while the number density of particles is fixed. The theoretical curve for hard spheres drawn using the Krieger-Dougherty model<sup>36</sup> is shown as the solid line for comparison.

In the blends, the number ratio of large:small particles was fixed at  $N_L:N_S = 1:800$  (equivalent to 70 wt% small particles), and the initial solids contents of the dispersions were fixed at *ca.* 10 wt%. It is important to clarify that both large and small particles are charge-stabilized over the entire pH range studied here. With a negative surface charge, which increases with increasing pH (Figure S2), they are subject to charge repulsion that imparts colloidal stability.

The structures of dried films were non-invasively probed using confocal laser scanning microscopy with two excitation wavelengths. These measurements allow the reconstruction of a 3D image of the distributions of the two kinds of particles. As is shown in Figure 3a-b (left column), for an initial dispersion pH of 3 and 4, a layer of green (small) particles is clearly seen at the top of the coating, whereas below the surface layer, red (large) particles predominate. The integrated intensity profiles (right column), which are proportional to the particle concentration, show peaks in the green channel intensity near the top surface, and thus provides unequivocal evidence for stratification. (The method of data reduction is explained in the Supporting Information.) The thickness of the upper layer is about 2  $\mu\text{m}$ , which is equivalent to *ca.* 40 diameters of the small particles.

When the pH of the initial dispersion is raised to 7 and beyond (Figures 3c-d), there is no evidence for stratification within the dried films. In fact, the intensities of both the red and green channels are seen to follow each other almost exactly, as is shown in the integrated intensity 1D profiles (right column). There is a broadening of the step in the intensity at the film surface because of the combined effects of imperfect sample levelling and fluctuations in thickness.

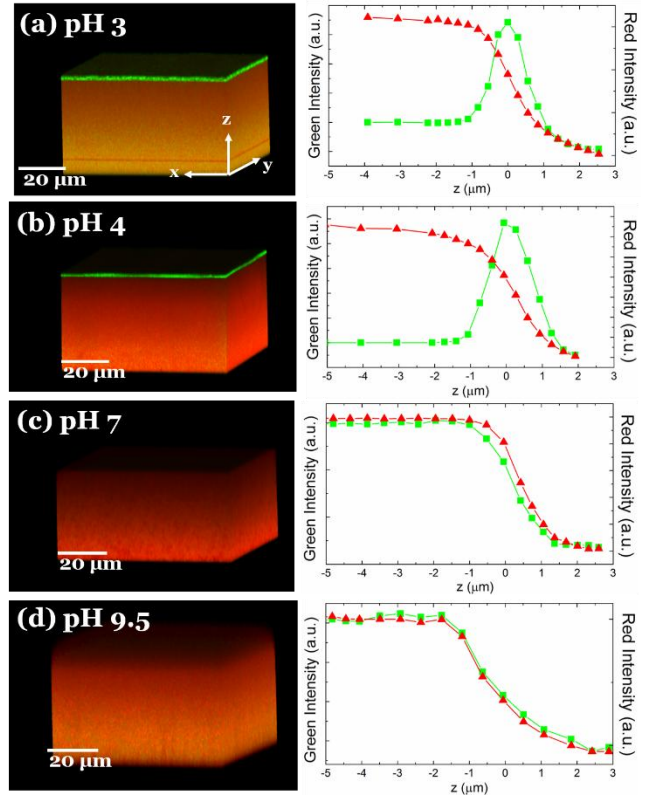


**Figure 3. Confocal laser scanning microscopy of dried films formed from a binary mixture of large particles and small pH-responsive particles, with number ratio of  $N_L:N_S = 1:800$  and an initial solids content of 10 wt%. Large particles are labeled with a red fluorescent dye, and small pH-responsive particles are labeled with a green dye. The left column shows three-dimensional confocal reconstructions of the dried films, obtained from for four different pH values of the initial dispersion: (a) pH 3, (b) pH 4, (c) pH 7 and (d) pH 9.5. The right column shows the integrated intensities of red (red triangles) and green (green squares) channels close to the top surface, as a function of the vertical distance,  $z$ . The surface is represented at  $z = 0$  as the center of the broadened step in intensity. A correction was made for the depth dependence of the detected fluorescence intensity.**

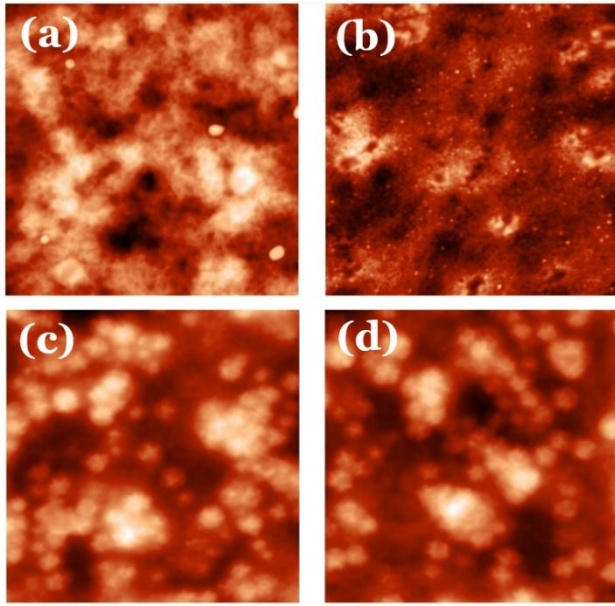


**Figure 4. Atomic Force Microscopy (AFM) of dried films formed from a binary mixture of large particles and small pH-responsive particles, with number ratio of  $N_L:N_S = 1:800$  and an initial solids content of 10 wt%. Height images ( $5 \times 5 \mu\text{m}^2$ ) obtained from for four different pH values of the initial dispersion: (a) pH 3, (b) pH 4, (c) pH 7 and (d) pH 9.5.**

To verify this transition in stratification, the top surface of the final films was characterized by means of atomic force microscopy (AFM) as can be seen in Figures 4a-d. At low pH, the top surface of the film is covered with small particles and just a few large ones can be visualized (Figures 4a-b). This is consistent with a picture of a stratified coating where small particles accumulate at the top, with the large ones below. However, for pH 7 and above, numerous large particles can be seen at the top surface (Figures 4c-d). The AFM images indicate a transition from a stratified to a non-stratified coating at pH around 7. (Although the small particles swell in alkaline water, they will collapse upon drying and film formation.)

To shed light on the effect of reduced particle mobility on stratification, we carried out Langevin dynamics simulations<sup>37</sup> of drying films with a binary mixture of large and small spherical particles. The mixtures all had number ratios of large to small particles of  $N_L:N_S = 1:800$  to match the experiments. Screened charged particles were assumed. The model is described in the Supporting Information and in detail elsewhere.<sup>16</sup> Briefly, we started with a size ratio between the large and small particles of  $D_L:D_S = 7:1$ , which corresponds to the effective size ratio in experiments at low pH. We then increased  $D_S$ , keeping the  $D_L$  and the number densities of the particles the same, to model the swelling of the small particles with increasing pH.

The initial volume fraction occupied by the particles in the simulation increased from 0.1 to 0.55, with increasing  $D_S$ . When the small particles are 54 nm in diameter (Figure 5a), they accumulate in a top layer, and the system is

stratified. But when  $D_S$  increases, the stratification disappears (Figure 5b). Indeed, Figure 6a shows that the width of the layer of small particles falls towards zero when their diameter is above approximately 80 nm, which is very close to the diameter where stratification is lost in the experiments (Figures 2a and 3c). We note that halving the initial number densities of the particles did not cause the stratification effect to return, just as it did not in the experiments (Figure S7).

In earlier work,<sup>16</sup> we found that stratification occurred because the larger particles moved down faster than the small particles during drying. We estimated that the excess velocity of the large particles over that of the small particles scales approximately as the product of the square of the size ratio and the pressure gradient; it scales inversely with the suspension viscosity. (See Equation S3.) As the pH increases in our experiments, the size of small particle increases. Our simulations show that as  $D_S$  increases with the number of particles constant, the segregation mechanism is hindered by four effects. Three of these effects reduce the relative downward velocities of the large and small particles. It is this relative motion that drives the segregation. Firstly, the size ratio decreases from 7:1 to approximately half that value, and the relative motion tends to zero as the size ratio tends toward unity. Secondly, the initial  $\phi_{\text{eff}}$  increases, which leads to an increased suspension viscosity. Thirdly, the pressure gradients decrease, as shown in Figure S8, reducing the velocity difference between the particles. Fourthly, the time available before jamming of the particles decreases. Hence, with a larger  $D_S$ , the particles jam before they have finished stratifying. This effect is represented in the map in Fig. 6b, which identifies the region (shaded green) where particles are not jammed and can stratify. A drying film follows vertical time trajectories in this figure.

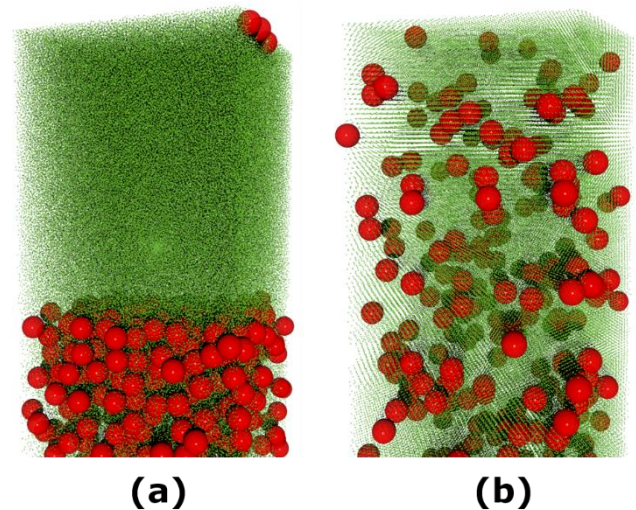


**Figure 5. (a), (b) Simulation snapshots at the end of drying runs, showing the top 30% of the simulation box. Large and small particles are red and green, respectively. For clarity in the visualization, we present the small particles as having a diameter 1/70 of the large particle**

diameter,  $D_L = 385$  nm. In (a)  $D_S = 54$  nm and the size ratio  $D_L:D_S = 7:1$ . In (b)  $D_S = 97$  nm and the size ratio is 4:1. Snapshot (a) is from a run with an initial volume fraction occupied by the spheres is  $\phi_0 = 0.1$ , while in (b) the number density is the same, but swelling of the small particles increases  $\phi_0$  to 0.45. Further details of the simulations are given in the Supporting Information.

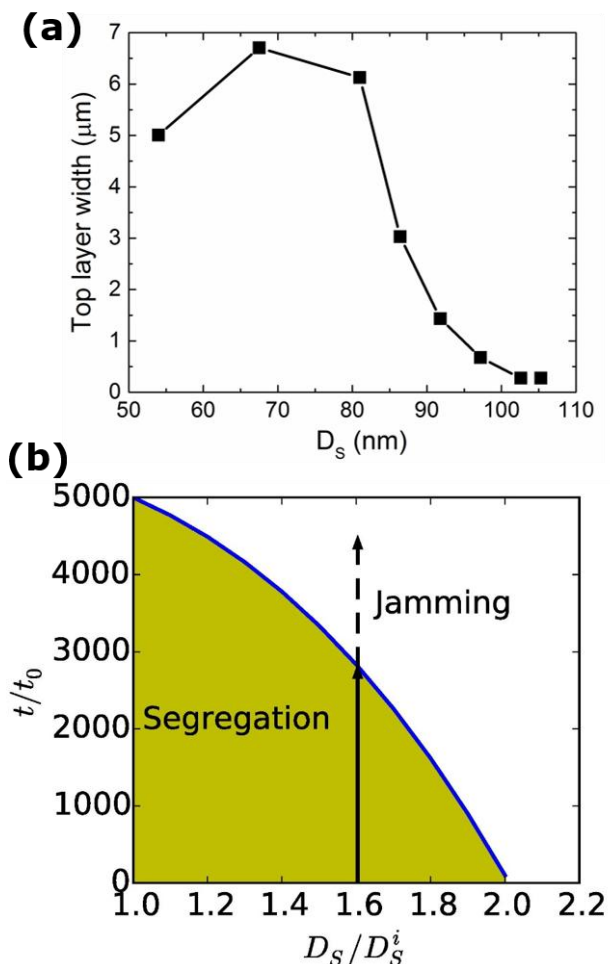


**Figure 6.** (a) Width of the stratified top layer of small particles, as a function of their diameter. (b) The sketch shows the dynamic region where segregation is possible (green shaded area) and where jamming occurs (white area).  $D_S$  is normalized by the initial size without swelling,  $D_S^i$ ; the time is normalized by the simulation time unit,  $t_0$ . The full curve denotes the elapsed normalized time until an average volume fraction of 60% is reached. Evaporation corresponds to moving vertically in the plane. The vertical arrow indicates an example drying path. The solid arrow shows the part of the dynamic path where segregation is possible. Further details of the simulations are given in the Supporting Information.

**Conclusions.** To summarize, we have demonstrated a bimodal colloidal system that allows self-stratification during drying to be switched off using pH as the trigger. Coatings are stratified when cast from dispersion with a

pH below 7, but the effect is lost at higher pHs. Our stimuli-responsive polymer colloids increase in size when the pH is raised. We carried out simulations that showed that when the particle size increases above 80 nm, the stratification is suppressed, which agrees remarkably well with the experiments. These simulations allowed us to determine the mechanism that controls stratification and to explain the observed switchability.

Achieving such control over the stratification process allows not only the independent programming of the properties of the top surface, but also the possibility of switching the surface properties without changing the starting materials. Our design potentially provides a means to change – whenever desired – the hardness and optical reflectivity of a coating during deposition.

Our concept has significant potential for a wide range of applications, especially smart paints and inks. The stratification control could also be used to tailor the tack strength of pressure-sensitive adhesives.<sup>23</sup> Although our focus here is on switchable stratification, our insights into the effects of particle size and concentration on the stratification of binary particle blends can be exploited to achieve homogeneous coatings.

## Materials and Methods

**Particle synthesis and characterization.** The large Rhodamine B (RhB)-labeled latex particles (solids content of 20.6 wt%) were produced by emulsion copolymerization of methyl methacrylate and *n*-butyl acrylate (40 : 60 g/g) using sodium persulfate (0.5 wt% relative to monomers) as initiator and a combination of non-ionic and anionic surfactants (99 : 1 g/g), Synperonic NP30 and sodium dodecyl sulfate, respectively. The polymerization was conducted in a batch process at 70 °C under a nitrogen atmosphere in a 300 mL glass reactor fitted with a condenser and a nitrogen gas inlet. Degassing of an aqueous solution of initiator was first carried out for 30 min. In the meantime, RhB (0.2 wt% based on monomers) was dissolved in a water solution containing the surfactants (3 g L<sup>-1</sup>). This solution was degassed, mixed with the monomers, and introduced in the reactor with vigorous stirring before increasing the temperature to start the polymerization. At the end of the reaction, the latex suspension was centrifuged, and fluorescence spectroscopy performed on the supernatant solution showed an extremely weak signal indicating that almost no RhB was present in the aqueous phase.<sup>38</sup> The hydrodynamic particle diameter was measured on dilute dispersions by DLS using a Malvern Zetasizer Nano ZS with a 633 nm wavelength laser and a scattering angle of 173°. These particles had a z-average diameter,  $D_L = 385$  nm with a dispersity of 0.013 (PDI value). The copolymer's midpoint glass transition temperature was 11 °C, according to differential scanning calorimetry (Q1000, TA Instruments, New Castle, DE, USA) at 10 °C/min. Film formation could occur at a typical room temperature.

The small fluorescent particles were composed of amphiphilic block copolymers obtained by polymeriza-

tion-induced self-assembly (PISA).<sup>34, 35</sup> Controlled radical polymerization (namely, reversible addition-fragmentation chain transfer (RAFT) polymerization) of methacrylic acid (MAA) in water was performed to obtain, firstly, a PMAA macroRAFT agent (about 4000 g mol<sup>-1</sup>),<sup>39</sup> which was then chain-extended with a mixture of *n*-butyl acrylate, styrene and fluorescein *o*-acrylate (54.9/44.7/0.4 wt%) in a H<sub>2</sub>O/EtOH mixture (90/10 v/v). 4,4'-Azobis(4-cyanopentanoic acid) (ACPA) was used as an initiator with [ACPA]<sub>H<sub>2</sub>O/EtOH</sub> = 2.2 mmol L<sup>-1</sup> and [PMAA]/[ACPA] = 4.9. After the synthesis, the stable polymer dispersion was degassed under argon to remove traces of *n*-butyl acrylate. It was also dialyzed against water over 69 h, thus allowing the removal of ethanol in the final dispersion. The final solids content was 20.9 wt%. DLS found  $D_s = 54$  nm with a PDI value of 0.065 at an initial pH of 4. At this pH, which is below PMAA's pK<sub>a</sub> value of 5.5, the PMAA chains at the particle surface are only weakly ionized and likely adopt a hypercoiled conformation.<sup>40</sup> The copolymer's midpoint glass transition temperature was 16 °C, according to differential scanning calorimetry at 10 °C/min.

**Blend preparation and drying.** After blending the two dispersions to achieve the desired number ratio, deionized water was added to adjust the final solids content to the range from 9 to 13 wt%. By adding small amounts of ammonia (35 %) or 1M HCl solution the pH of the blend was adjusted to pH values between 3 and 9.5. The pH of the colloidal mixture was estimated using pH indicator paper, because of the small sample volume. Films of these blends were cast on glass substrates (18 × 18 mm<sup>2</sup>), previously cleaned with acetone and a UV ozone treatment (Bioforce Nanosciences, model UV.TC.EU.003). Film formation took place under ambient conditions (typically a temperature of 20 °C and a relative humidity of 40%). Average drying times were 1-2 h.

**Structure characterization.** Height and phase images of the top surface of the films were acquired by atomic force microscopy (AFM), using an NT-MDT Ntegra Prima microscope with intermittent contact. Images were analyzed using NOVA software. A Zeiss LSM510 confocal microscope (on an Axiovert 200M microscope) was used to obtain stacks of plane images at varying depths within the sample. The green and red fluorochromes were excited using an argon laser (488 nm) and a HeNe laser (543 nm), respectively. Two-dimensional images (83 × 83 μm<sup>2</sup>) were acquired in 0.5 μm increments when moving from the substrate at the bottom toward the top of the dry film. A second acquisition was made close to the top surface to characterize the upper layer with greater precision, acquiring images with increments in spacing of 0.1 μm. Results were analysed using the image processing package Fiji (a version of Image J). A second-order polynomial equation was fit to the detected intensity as a function of depth from the surface and then used to define a baseline, to correct for the depth-dependence of the detected intensity. The corrected intensity was normalized by divid-

ing by the maximum intensity in the profile. An example can be seen in the Supporting Information.

**Dispersion viscosity measurements.** The viscosities of the large and small particle dispersions containing 20 wt% solids were determined over the pH range from 2.5 to 9.5. Small amounts of concentrated aqueous ammonia (35 %) or 1M HCl solutions were used to adjust the original pH, in order to minimize changes to the particle concentration. Viscosity measurements were made on ~0.8 mL of each dispersion at ambient temperature (24 ± 2 °C) using a low-shear rheometer (Contraves A.G., Zürich, Switzerland) with concentric cylinder measuring geometry over a range of shear rates.

## ASSOCIATED CONTENT

**Supporting Information.** Hydrodynamic diameters of large particles by DLS; zeta potential measurements of large and small particles; shear rheology; visible absorption spectra of fluorescent particles; 3D confocal reconstructions of films at pH 3.5 and 8; analysis of confocal laser scanning images; information on Langevin dynamics simulations. This material is available free of charge via the Internet at <http://pubs.acs.org>.

## AUTHOR INFORMATION

### Corresponding Author

\* E-mail: J.Keddie@Surrey.ac.uk

### Present Addresses

†Department of Materials, Loughborough University, Loughborough, Leicestershire, LE11 3TU, UK.

### Author Contributions

The manuscript was written through contributions of all authors. All authors have given approval to the final version of the manuscript.

### Funding Sources

European Union Seventh Framework Programme BARRIER-PLUS project (FP7-SME-2012-2, No. 304758).

## ACKNOWLEDGMENT

This work was funded by the European Union Seventh Framework Programme BARRIER-PLUS project (FP7-SME-2012-2, No. 304758). We thank Dr Rachel E. Butler at the University of Surrey Bioimaging and Flow Cytometry Core Facility for assistance with confocal microscopy experiments and Violeta Doukova (University of Surrey) for general laboratory support.

## REFERENCES

- (1) Xu, Q.; Lv, Y.; Dong, C.; Sreepredas, T. S.; Tian, A.; Zhang, H.; Tang, Y.; Yu, Z.; Li, N. Three-dimensional micro/nanoscale architectures: fabrication and applications. *Nanoscale* **2015**, *7*, 10883-10895.
- (2) Lee, I.; Park, J. Y.; Gim, S.; Kim, K.; Cho, S. H.; Choi, C. S.; Song, S. Y.; Lee, J. L. Optical Enhancement in Optoelectronic Devices Using Refractive Index Grading Layers. *ACS Appl. Mater. Interfaces* **2016**, *8*, 3326-3332.

- (3) Zervantonakis, I. K.; Arvanitis, C. D. Controlled Drug Release and Chemotherapy Response in a Novel Acoustofluidic 3D Tumor Platform. *Small* **2016**, *2616-2626*.
- (4) Xu, B.; Zheng, Z.; Zhao, K.; Hou, J. A Bifunctional Interlayer Material for Modifying Both the Anode and Cathode in Highly Efficient Polymer Solar Cells. *Adv. Mater.* **2016**, *28*, 434-439.
- (5) Hammond, P. T. Form and function in multilayer assembly: New applications at the nanoscale. *Adv. Mater.* **2004**, *16*, 1271-1293.
- (6) Richardson, J. J.; Bjornmalm, M.; Caruso, F. Multilayer assembly. Technology-driven layer-by-layer assembly of nanofilms. *Science* **2015**, *348*, aaa2491.
- (7) Steiner, U.; Klein, J.; Eiser, E.; Budkowski, A.; Fetters, L. J. Complete wetting from polymer mixtures. *Science* **1992**, *258*, 1126-1129.
- (8) Geoghegan, M.; Jones, R. A. L.; Payne, R. S.; Sakellariou, P.; Clough, A. S.; Penfold, J. Lamellar structure in a thin polymer blend film. *Polymer* **1994**, *35*, 2019-2027.
- (9) Coveney, S.; Clarke, N. Pattern Formation in Polymer Blend Thin Films: Surface Roughening Couples to Phase Separation. *Phys. Rev. Lett.* **2014**, *113*, 218301.
- (10) Heriot, S. Y.; Jones, R. A. L. An interfacial instability in a transient wetting layer leads to lateral phase separation in thin spin-cast polymer-blend films. *Nat. Mater.* **2005**, *4*, 782-786.
- (11) Nikiforow, I.; Adams, J.; König, A. M.; Langhoff, A.; Pohl, K.; Turshatov, A.; Johannsmann, D. Self-Stratification During Film Formation from Latex Blends Driven by Differences in Collective Diffusivity. *Langmuir* **2010**, *26*, 13162-13167.
- (12) Trueman, R. E.; Lago Domingues, E.; Emmett, S. N.; Murray, M. W.; Routh, A. F. Auto-stratification in drying colloidal dispersions: A diffusive model. *J. Colloid Interface Sci.* **2012**, *377*, 207-212.
- (13) Cardinal, C. M.; Jung, Y. D.; Ahn, K. H.; Francis, L. F. Drying regime maps for particulate coatings. *AIChE J.* **2010**, *56*, 2769-2780.
- (14) Atmuri, A. K.; Bhatia, S. R.; Routh, A. F. Autostratification in Drying Colloidal Dispersions: Effect of Particle Interactions. *Langmuir* **2012**, *28*, 2652-2658.
- (15) Misra, A.; Jarrett, W. L.; Urban, M. W. Fluoromethacrylate-Containing Colloidal Dispersions: Phospholipid-Assisted Synthesis, Particle Morphology, and Temperature-Responsive Stratification. *Macromolecules* **2007**, *40*, 6190-6198.
- (16) Fortini, A.; Martin-Fabiani, I.; De La Haye, J. L.; Dugas, P.-Y.; Lansalot, M.; D'Agosto, F.; Bourgeat-Lami, E.; Keddie, J. L.; Sear, R. P. Dynamic Stratification in Drying Films of Colloidal Mixtures. *Phys. Rev. Lett.* **2016**, *116*, 118301.
- (17) Nunes, J. S.; Bohórquez, S. J.; Meeuwisse, M.; Mestach, D.; Asua, J. M. Efficient strategy for hard nano-sphere usage: Boosting the performance of waterborne coatings. *Prog. Org. Coat.* **2014**, *77*, 1523-1530.
- (18) Chhajed, S.; Schubert, M. F.; Kim, J. K.; Schubert, E. F. Nanostructured multilayer graded-index antireflection coating for Si solar cells with broadband and omnidirectional characteristics. *Appl. Phys. Lett.* **2008**, *93*, 251108.
- (19) Yu, E. T.; van de Lagemaat, J. Photon management for photovoltaics. *MRS Bull.* **2011**, *36*, 424-428.
- (20) Goldstein, L.; Glas, F.; Marzin, J. Y.; Charasse, M. N.; Leroux, G. Growth by molecular-beam epitaxy and characterization of INAs/GaAs strained-layer superlattices. *Appl. Phys. Lett.* **1985**, *47*, 1099-1101.
- (21) Choy, K. L. Chemical vapour deposition of coatings. *Prog. Mater. Sci.* **2003**, *48*, 57-170.
- (22) Jensen, J. M.; Oelkers, A. B.; Toivola, R.; Johnson, D. C.; Elam, J. W.; George, S. M. X-ray reflectivity characterization of ZnO/Al<sub>2</sub>O<sub>3</sub> multilayers prepared by atomic layer deposition. *Chem. Mater.* **2002**, *14*, 2276-2282.
- (23) Gurney, R. S.; Dupin, D.; Nunes, J. S.; Ouzineb, K.; Siband, E.; Asua, J. M.; Armes, S. P.; Keddie, J. L. Switching Off the Tackiness of a Nanocomposite Adhesive in 30 s via Infrared Sintering. *ACS Appl. Mater. Interfaces* **2012**, *4*, 5442-5452.
- (24) Fortini, A.; Sear, R. *Langmuir* **2016**. Submitted.
- (25) Stuart, M. A. C.; Huck, W. T. S.; Genzer, J.; Muller, M.; Ober, C.; Stamm, M.; Sukhorukov, G. B.; Szleifer, I.; Tsukruk, V. V.; Urban, M.; Winnik, F.; Zauscher, S.; Luzinov, I.; Minko, S. Emerging applications of stimuli-responsive polymer materials. *Nat Mater* **2010**, *9*, 101-113.
- (26) Progress in Organic Coatings Zhang, P. H.; Wang, C.; Zhao, J. J.; Xiao, A. Q.; Shen, Q.; Li, L. T.; Li, J. X.; Zhang, J. F.; Min, Q. H.; Chen, J. N.; Chen, H. Y.; Zhu, J. J. Near Infrared-Guided Smart Nanocarriers for MicroRNA-Controlled Release of Doxorubicin/siRNA with Intracellular ATP as Fuel. *ACS Nano* **2016**, *10*, 3637-3647.
- (27) Kim, J.-H.; Jung, Y.; Lee, D.; Jang, W.-D. Thermoresponsive Polymer and Fluorescent Dye Hybrids for Tunable Multicolor Emission. *Adv. Mater.* **2016**, *28*, 3499-3503.
- (28) Epstein, E.; Yoon, J.; Madhukar, A.; Hsia, K. J.; Braun, P. V. Colloidal Particles that Rapidly Change Shape via Elastic Instabilities. *Small* **2015**, *11*, 6051-6057.
- (29) Asua, J. M. Emulsion polymerization: From fundamental mechanisms to process developments. *J. Polym. Sci., Part A: Polym. Chem.* **2004**, *42*, 1025-1041.
- (30) De Bruyn, H.; Gilbert, R. G.; White, J. W.; Schulz, J. C. Characterization of electrosterically stabilized polystyrene latex; implications for radical entry kinetics. *Polymer* **2003**, *44*, 4411-4420.
- (31) Charleux, B.; D'Agosto, F.; Delaittre, G., Preparation of Hybrid Latex Particles and Core-Shell Particles Through the Use of Controlled Radical Polymerization Techniques in Aqueous Media. *Adv Polym Sci* **2010**, *233*, 125-183.
- (32) Xie, J.; Nakai, K.; Ohno, S.; Butt, H.-J.; Koynov, K.; Yusa, S.-i. Fluorescence Correlation Spectroscopy Monitors the Hydrophobic Collapse of pH-Responsive Hairy Nanoparticles at the Individual Particle Level. *Macromolecules* **2015**, *48*, 7237-7244.
- (33) Charleux, B.; Delaittre, G.; Rieger, J.; D'Agosto, F. Polymerization-Induced Self-Assembly: From Soluble Macromolecules to Block Copolymer Nano-Objects in One Step. *Macromolecules* **2012**, *45*, 6753-6765.
- (34) Canning, S. L.; Smith, G. N.; Armes, S. P. A Critical Appraisal of RAFT-Mediated Polymerization-Induced Self-Assembly. *Macromolecules* **2016**, *49*, 1985-2001.
- (35) Lansalot, M.; Rieger, J.; D'Agosto, F., Polymerization-Induced Self-Assembly: the Contribution of Controlled Radical Polymerization to the Formation of Self-Stabilized Polymer Particles of Various Morphologies. In *Macromolecular self-assembly*, O, B.; L, B., Eds.; **2016**.
- (36) Krieger, I. M.; Dougherty, T. J. A Mechanism for Non - Newtonian Flow in Suspensions of Rigid Spheres. *Trans. Soc. Rheol.* **1959**, *3*, 137-152.
- (37) Plimpton, S. Fast Parallel Algorithms for Short-Range Molecular Dynamics. *J. Comput. Phys.* **1995**, *117*, 1-19.
- (38) Soleilhac, A.; Girod, M.; Dugourd, P.; Burdin, B.; Parvole, J.; Dugas, P.-Y.; Bayard, F.; Lacôte, E.; Bourgeat-Lami, E.; Antoine, R. Temperature Response of Rhodamine B-Doped Latex Particles. From Solution to Single Particles. *Langmuir* **2016**, *32*, 4052-4058.
- (39) Chaduc, I.; Lansalot, M.; D'Agosto, F.; Charleux, B. RAFT Polymerization of Methacrylic Acid in Water. *Macromolecules* **2012**, *45*, 1241-1247.
- (40) Ruiz-Perez, L.; Pryke, A.; Sommer, M.; Battaglia, G.; Soutar, I.; Swanson, L.; Geoghegan, M. Conformation of poly(methacrylic acid) chains in dilute aqueous solution. *Macromolecules* **2008**, *41*, 2203-2211.

# TOC graphic

---

